JOURNAL OF MATERIALS SCIENCE 14 (1979) 1877–1889

Conductivity and creep in acceptor-dominated polycrystalline Al_2O_3

L. D. HOU, S. K. TIKU, H. A. WANG, F. A. KRÖGER
Department of Materials Science, University of Southern California, Los Angeles, California 90007, USA

Ionic and electronic conductivity and compressive creep of hot-pressed polycrystalline acceptor-dominated Al_2O_3 were measured as a function of oxygen partial pressure and grain size varying from 3 to 200 μm. Hole conduction shows a slight preference for grain-boundaries; ionic conduction is slightly hindered by grain boundaries, indicating that fast oxygen grain-boundary diffusion involving charged species does not occur. Conductivity and creep are accounted for on the basis of a model in which there is fast grain-boundary migration by a neutral oxygen species.

1. Introduction

It is generally accepted that sintering and diffusional creep of polycrystalline Al_2O_3 involve relatively rapid grain-boundary diffusion of oxygen, slower bulk diffusion of aluminium and possibly surface diffusion of aluminium. Expressions for an effective diffusion coefficient of Al_2O_3 have been derived which show how the rate of the overall diffusional process depends on the diffusion coefficients of Al and O [1, 2]. Deformation maps have been constructed which indicate that at low stresses, oxygen grain-boundary diffusion is rate-limiting at large grain sizes and high temperatures (Coble creep), aluminium lattice diffusion is rate-limiting at medium grain sizes and temperatures (Nabarro–Herring creep) and aluminium grain-boundary diffusion is rate-limiting at small grain sizes and low temperatures (Coble creep) [3, 4]. At high stresses, climb of dislocations (Harper–Dorn creep) becomes rate-limiting [4]. Doping with acceptors with a charge lower than that of Al (e.g. Fe^{2+}) affects the concentrations of native defects and therewith the self-diffusion of Al and O. Variation of the oxygen pressure changes the fraction of acceptor that is present in the aliovalent form and also the rate of creep and sintering [5]. Increased acceptor doping expands the region of creep limited by oxygen grain-boundary diffusion at the cost of that limited by Al bulk diffusion, indicating that acceptor doping affects Al bulk diffusion more strongly than it does O grain-boundary diffusion [4].

Work on single crystals has shown that doping with aliovalent ions also affects conductivity. Acceptor doping increases both hole conductivity (high p_{O_2}) and ionic conductivity (V_O^{2+} and/or Al_i^{3+}, low p_{O_2}) [6–8]; donor doping increases both electron conductivity (low p_{O_2}) and ionic conductivity (V_{Al}^{3+}, high p_{O_2}) [9].

It is of interest to investigate how the conductivity of polycrystalline Al_2O_3 is affected by doping and oxygen pressure and if and how this conductivity varies with grain size. This is done by making samples of the same composition with different grain sizes. Creep is measured for the same samples. A detailed model explaining almost all the results is presented. Since ionic and electronic conduction may depend on grain size in a different manner, the study was carried out for each of these under conditions where it is dominant.

2. Experimental procedures

2.1. Sample preparation

Al_2O_3 powders were made from analytical grade $Al_2(SO_4)_3 \cdot 18H_2O$ by the following method. The sulphate is dissolved in de-ionized water and then precipitated by pouring the solution into water-free acetone. The precipitate is separated by filtration, then dried and decomposed to $\gamma \cdot Al_2O_3$ by calcination for 5 hours at 850° C. Samples doped with Fe or Ti are made in a similar way by adding the required amount of $FeSO_4$ or $TiCl_4$ to the sulphate solution before precipitation. The

0022–2461/79/081877–13 $03.30/0

TABLE I

Sample composition	Hot pressed, 4500 psi		Sintered		Grain size d	Density % theoretical, 3.986
	(° C)	(h)	(° C)	(h)		
undoped	1450	½	1500	48	3	99.5
			1600	120	10	
			1700	72	20	
	1600	1	1500	48	100	99.9
: 80 ppm Ti	1450	½	1500	48	6	99.4
: 500 ppm Fe	1450	½	1500	48	3	
			1600	120	12	98.1
			1700	72	25	
: 5000 ppm Fe	1450	½	1500	48	10	99.8

powder is then outgassed by heating it at 1200° C in vacuum for 2 h. During this process, Al_2O_3 changes from γ to α form. Cylindrical samples of 2.5 cm diameter and 1 cm height were made by hot-pressing the powder in a graphite die for ½ h at 1550 to 1650° C *in vacuo* under a pressure of 4500 psi*.

The large samples were sectioned into smaller ones for the measurements: rectangular blocks of 6 mm × 3 mm × 3 mm for the creep measurements, and cylindrical plates of 12 mm diameter, 1 to 2 mm thickness for the electrical measurements. The samples were annealed at 1500° C for 2 to 7 days before the measurements to stabilize the microstructure. Density was determined by weighing with a pycnometer. Grain size, d, was determined from photographs of a polished and etched surface made under a metallographic microscope. The etchant used was hot H_3PO_4. Grain size was calculated from

$$d = 1.56L/NM$$

where L is the length of a line on the photograph, N the number of intercepts of the line with grain boundaries, and M the magnification [10]. Grain size was changed either by sintering or by preparation of fresh samples under different hot-pressing conditions. Table I summarizes the methods used for the preparation of the various samples and their grain size and density. Table II gives concentrations of impurities and dopants as determined by semiquantitative spectrographic analysis for undoped samples and for samples doped with 500 and 5000 ppm Fe and 80 ppm Ti.

2.2. Electrical measurements

Electrical conductivity was measured as a function of oxygen pressure and temperature in an apparatus as described in [6]. Surface and/or gas phase conduction was eliminated with the aid of a biased volume guard. For the experimental procedures see [6]. Ionic and electronic transference numbers $t_i = \sigma_i/\sigma$ and $t_{el} = 1 - t_i = \sigma_{el}/\sigma$ (where σ, σ_i, and σ_{el} are the total conductivity and its ionic and electronic components, with $\sigma = \sigma_i + \sigma_{el}$) were determined from measurements of the emf of cells

$$Pt, O_2, I/Al_2O_3/Pt, O_2, II.$$

Since

$$E = \frac{RT}{4F} \int_{p_{O_2,I}}^{p_{O_2,II}} t_i \, d \ln p_{O_2} \qquad (1)$$

$$(t_i)_{II} = \left\{ \partial \left(\frac{4F}{RT} \right) E \Big/ \partial \ln (p_{O_2})_{II} \right\} p_{O_2,I}. \qquad (2)$$

TABLE II Wt % of foreign element in Al_2O_3 samples

Element	Pure	500 ppm Fe-doped	5000 ppm Fe-doped	80 ppm Ti-doped
Ca	0.004 3	0.004 1	0.002 6	0.004
Co	ND < 0.000 4	0.002 1	ND < 0.000 4	ND < 0.000 4
Cr	ND < 0.000 2	0.001 9	0.001 5	0.000 56
Cu	0.000 072	0.000 073	0.000 58	0.000 50
Fe	0.001 6	0.048	0.42	0.011
Ga	ND < 0.002	0.005 6	0.006 7	0.010
Mg	0.002 0	0.006 4	0.006 5	0.006 3
Mn	ND < 0.002	0.006 9	0.007 7	TR < 0.001
Mo	0.004 6	ND < 0.000 4	0.004	ND < 0.000 4
Na	ND < 0.04	ND < 0.04	ND < 0.04	ND < 0.04
Ni	ND < 0.000 5	TR < 0.000 5	0.000 97	ND < 0.000 5
Pb	ND < 0.01	ND < 0.01	ND < 0.01	ND < 0.01
Si	0.007 2	0.008 6	0.010	0.023
Ti		ND < 0.001	ND < 0.001	0.007 9

*10^3 psi = 6.89 N mm^{-2}.

In order to prevent leakage of oxygen from one side of the cell to the other, p_{O_2} gradients which are too large are avoided by covering the O_2-pressure range in steps, e.g. from 1 to 10^{-5} atm and from 10^{-5} to 10^{-9} atm. Oxygen pressures were established with the aid of pure oxygen (1 atm), air (0.21 atm), technical nitrogen, monitored with a stabilized zirconia gauge (10^{-5} to 10^{-4} atm), and CO–CO_2 mixtures (10^{-5} to 10^{-9} atm). Again a volume guard is used to eliminate surface and gas phase conduction. For the exact procedures see [6] and [11].

2.3. Creep measurements

Compressive creep was measured in an apparatus according to the design by Cannon [12], modified to allow variation of oxygen partial pressure from 1 to 10^{-9} atm. Stresses of up to 50 NM m^{-2} were applied along the length of the 6 mm x 3 mm x 3 mm samples. Stress was applied with the aid of cylindrical SiC rods of 25 mm diameter. Single crystal sapphire plates of 45 mm x 10 mm x 6 mm and SiC discs (12 mm diameter, 3 mm thick) were used between the rods and the sample. The strain of the sample was transferred to the strain gauge through single crystal sapphire rods (3 mm diameter) resting on the sapphire plates. Strain was measured with a linear voltage differential transformer placed at the top of the furnace, and recorded with a Moseley Autograph 680 recorder. Temperatures up to 1550° C were established with a Pt–Rh furnace regulated to ±2° C with a Thermac 6000 Controller.

3. Experimental results

3.1. Conductivity and emf

Fig. 1 shows conductivity, σ, as $f(p_{O_2})$ for an undoped sample of grain size 3 μm at 1500° C, and the partial ionic and electronic conductivities $\sigma_i = t_i\sigma$ and $\sigma_{el} = t_{el}\sigma = (1 - t_i)\sigma$, using for t_i and t_{el} the values obtained from emf as $f(p_{O_2})$ shown in Fig. 2. The increase of σ_{el} with increasing p_{O_2} indicates that the sample is acceptor dominated, the partial electronic conductivity being a hole conductivity, $\sigma_{el} = \sigma_h$, with $\sigma_h = 5.8 \times 10^{-6}\, p_{O_2}^{1/4}\ \Omega^{-1}\ \mathrm{cm}^{-1}$. This oxygen pressure dependence is as expected for a model dominated by an acceptor with fixed valency, with either V_O^{2+} or Al_i^{3+} as the dominant native defect. The temperature dependence of σ at $p_{O_2} = 1$ atm where $\sigma \simeq \sigma_h$ and $p_{O_2} = 10^{-9}$ atm where $\sigma \simeq \sigma_i$ is shown in Fig. 3. There is little difference between curves

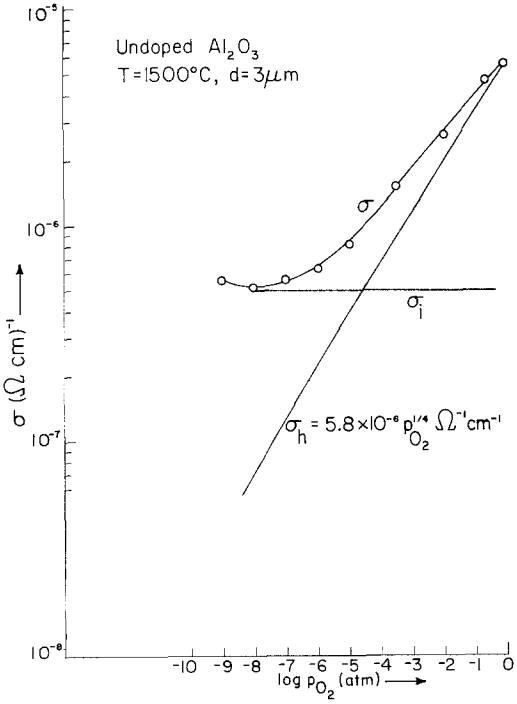

Figure 1 Conductivity σ and its ionic and electronic components σ_i and σ_h as $f(p_{O_2})$ (atm) for an undoped sample with $d = 3\,\mu$m at 1500° C.

measured in as short a time as possible, allowing no equilibration between sample and atmosphere ("non-equilibrium"), and those measured allowing a long time (= several hours) of equilibration ("equilibrium"). This is probably due to the fact that the acceptor has a fixed valency, a fact also indicated by the lack of a dependence of σ_i on p_{O_2}. The activation energy of hole conduction of 1.85 eV indicates that the separation between the acceptor level and the valence band has this value. The activation energy of σ_i of 3.78 eV should be

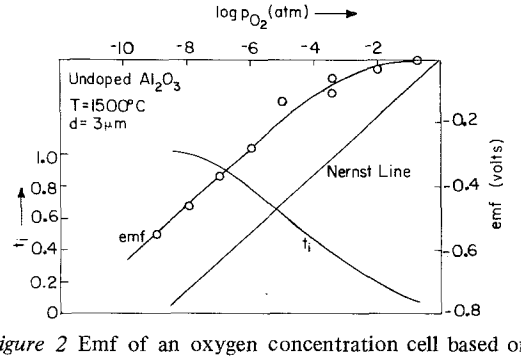

Figure 2 Emf of an oxygen concentration cell based on undoped polycrystalline Al_2O_3 with $d = 3\,\mu$m at 1500° C and the ionic transference numbers, t_i, deduced from it. The Nernst line, corresponding to $t_i = 1$, is shown for comparison.

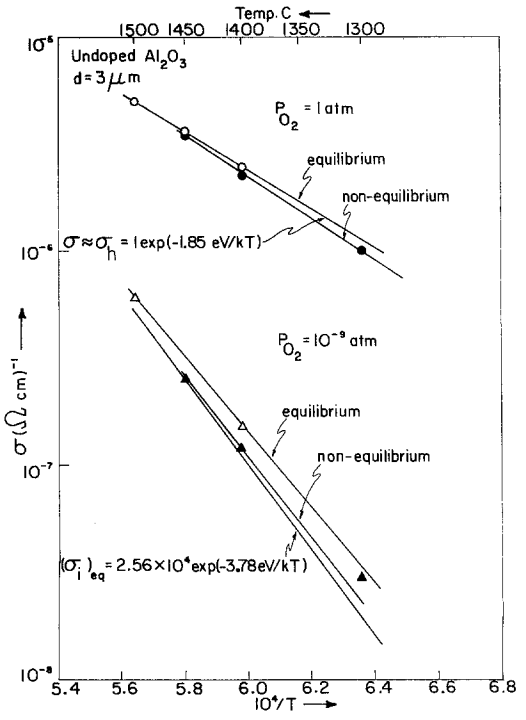

Figure 3 Temperature dependence of σ at $p_{O_2} = 1$ atm ($\sigma \approx \sigma_h$) and $p_{O_2} = 10^{-9}$ atm ($\sigma \approx \sigma_i$) for an undoped sample with $d = 3\,\mu$m, equilibrated and not equilibrated with the atmosphere.

the activation energy of the mobility of the ionic defect carrying the ionic current, V_O^{2+} or Al_i^{3+}. Figs. 4 and 5 show the conductivity, the emf, and t_i as a function of p_{O_2} at 1500° C for an undoped

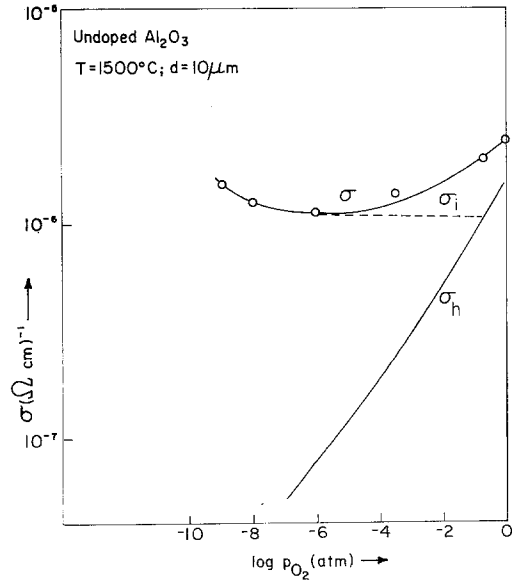

Figure 4 Conductivity σ and its components σ_i and σ_h as $f(p_{O_2})$ for undoped polycrystalline Al_2O_3 with grain size 10 μm at 1500° C.

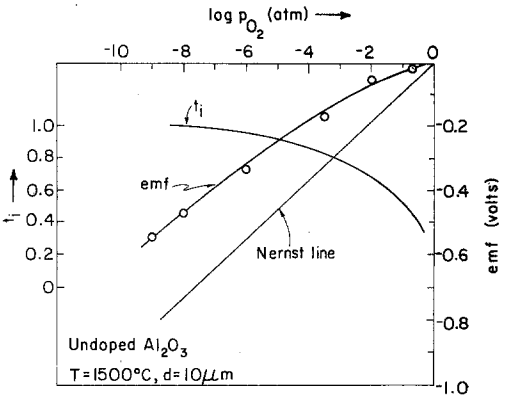

Figure 5 Emf of an oxygen concentration cell based on undoped polycrystalline Al_2O_3 with $d = 10\,\mu$m at 1500° C and the ionic transference numbers t_i deduced from it.

sample with grain size 10 μm. The sample is again acceptor dominated. That acceptor impurities are present in the undoped material is indicated by two further observations:

(1) after preparation by hot-pressing at 1650° C in the reducing atmospheres created by the graphite die, the samples are black. This blackening disappears upon oxidation and must be attributed to small metal particles (atom clusters) formed by reduction of an oxide different to Al_2O_3 (Al_2O_3 is not reduced under such conditions).

(2) Doping with 500 ppm Fe ($\simeq 2.1 \times 10^{19}$

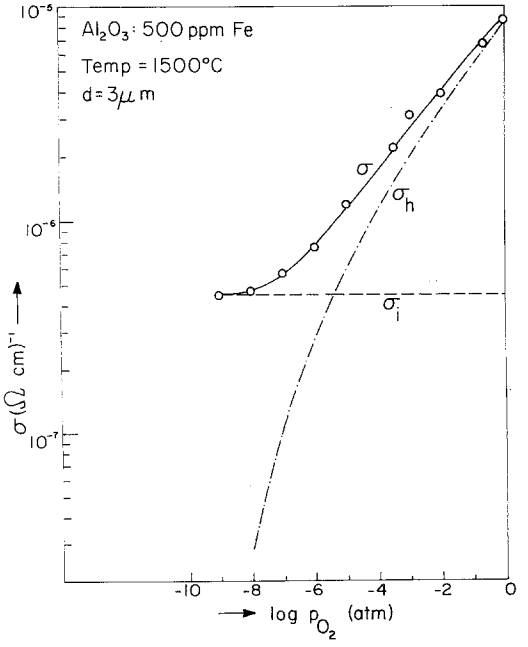

Figure 6 Conductivity σ and its components σ_i and σ_h as $f(p_{O_2})$ for Al_2O_3 doped with 500 ppm Fe at 1500° C; grain size $d = 3\,\mu$m.

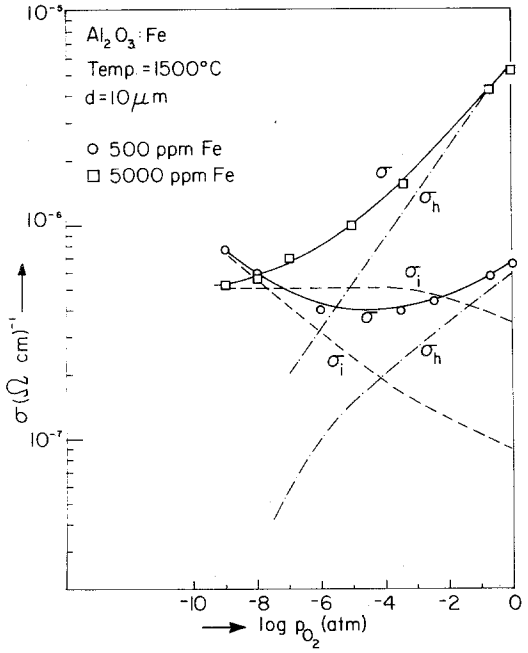

Figure 7 Conductivities σ and their components σ_i and σ_h as $f(p_{O_2})$ at 1500° C for samples doped with 500 and 5000 ppm Fe; $d = 10\,\mu m$.

(Fig. 6), which also does not show the expected cm^{-3}) has only a small effect on the conductivity dependence on p_{O_2} due to oxidation–reduction Fe^{2+}, Fe^{3+}. As seen in Fig. 7. Even doping with 5000 ppm Fe, though causing a more marked increase in σ, gives $\sigma_i \propto p_{O_2}^{0.1}$, with an exponent much smaller than expected for an Fe-dominated sample ($3/16 \simeq 0.188$ for $[Fe_{Al}^{-}] \simeq 3[Al_i^{3+}]$, $1/6 \simeq 0.167$ for $[Fe_{Al}^{-}] \simeq 2[V_O^{2+}]$). It should, of course, be remembered that only a fraction of the iron added is present as Fe^{2+}, most of it being Fe^{3+} and without effect on the concentration of native defects.

The amount of acceptor present was determined by "titration" with a donor, Ti. Samples doped with 20 ppm Ti ($\simeq 10^{18}$ cm^{-3}) are still acceptor dominated, but samples doped with 80 ppm Ti ($\simeq 4 \times 10^{18}$ cm^{-3}) are donor dominated (Figs. 8 and 9). At 1400° C the conductivity of the latter sample is almost purely ionic at all p_{O_2}, but at 1000° C it is ionic at high p_{O_2} and electronic (with $\sigma = \sigma_e$) at low p_{O_2}. From these observations, it may be concluded that the undoped sample contains $(2.5 \pm 1.5) \times 10^{18}$ acceptors cm^{-3}. The observed acceptor level position ($E_v + 1.9$ eV) is almost exactly that reported for Mg [8] and a similar level position may be expected for Ca. However, it is unlikely that oxides of these

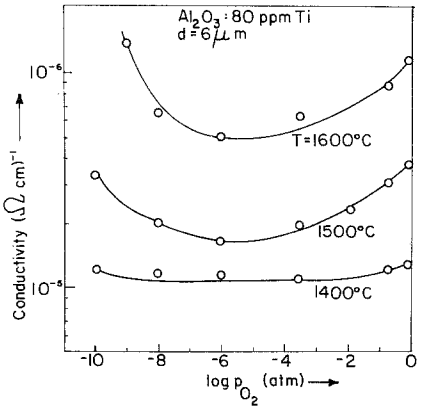

Figure 8 Oxygen pressure dependence of conductivity for samples doped with 80 ppm Ti (grain size 6 μm) at 1400, 1500 and 1600° C.

elements can be reduced to metal under the conditions of preparation. Table II shows, however, that Fe as well as Mg and Ca are present in the undoped material in concentrations of 6.8×10^{17}, 2×10^{18}, and 2.6×10^{18} cm^{-3}. It seems, therefore, that Mg (and possibly Ca) are the dominant acceptors, while Fe is responsible for the black colour of reduced samples. Note that Ca is usually found segregated at grain boundaries [13, 14] where it may, but need not, affect the conductivity. Mg segregates to a smaller extent [14–16].

The grain-size dependence of σ_h and σ_i for undoped samples and samples doped with 500 ppm Fe is shown in Figs. 10 and 11. The σ_h values were measured at 1 atm O_2, the σ_i values were taken from the flat parts of the $\sigma_i \therefore p_{O_2}$ curves.

The hole conduction decreases with increasing grain size up to $d = 10\,\mu m$ and becomes independent of grain size at larger ds. The ionic conductivity of the undoped samples shows the opposite behaviour, increasing with d up to $10\,\mu m$, de-

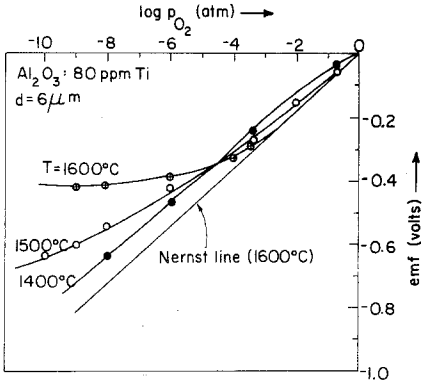

Figure 9 Emf as $f(p_{O_2})_{II}$ for a cell based on Al_2O_3: 80 ppm Ti at 1400, 1500 and 1600° C.

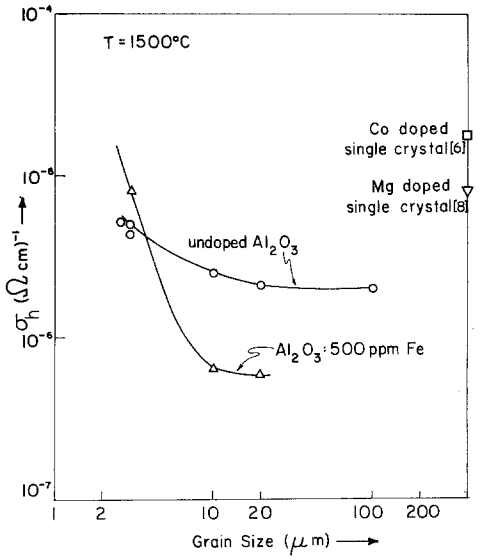

Figure 10 Grain size dependence of σ_h (measured at $p_{O_2} = 1$ atm) for undoped Al_2O_3 and Al_2O_3 doped with 500 ppm Fe. Single crystal values for crystals doped with Mg and Co are shown for comparison.

creasing at larger ds. For the Fe doped samples, σ_i is independent of d.

Fig. 11 also shows single crystal values for Al_2O_3:Mg [8] corrected for the differences in acceptor content (3.7×10^{17} cm^{-3} in the single crystal, 2.5×10^{18} cm^{-3} in the undoped sample). The correction is slightly different for the V_O^{2+} model ($\propto [Mg]^{1/2}$) and the Al_i^{3+} model ($\propto [Mg]^{3/4}$). These points are well in line with the data for undoped large-grain polycrystalline material. A corresponding value for Al_2O_3: 10^{18} cm^{-3} Co, 2×10^{-5} Ω^{-1} cm^{-1} [6] is a factor of $\simeq 10$ higher. There is no decrease of ionic conductivity with increasing grain size as expected in the presence of a considerable grain-boundary contribution to σ_i. Thus neither O nor Al migrate via grain boundaries in charged form. Yet grain-boundary diffusion by neutral species (which do not affect conductivity) may still be present. The decrease of σ_h with increasing d at small ds indicates increased hole transport via grain boundaries; a similar observation was reported for undoped and Mg-doped Al_2O_3 by Kitazawa and Coble [17]. The nature of the extra conductivity in polycrystalline Al_2O_3 reported by Özkan and Moulson [18] is unknown.

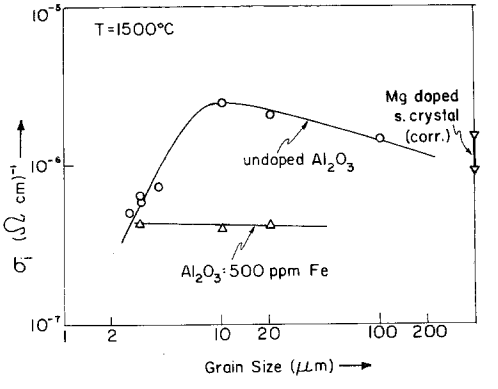

Figure 11 Ionic conductivity as f (grain size, d) for undoped Al_2O_3 and Al_2O_3 doped with 500 ppm Fe. Corrected single-crystal values for Mg and Co are shown for comparison.

The fact that the decrease of σ_h and the increase of σ_i with increasing d is observed only at $d \leqslant 10\,\mu$m may have two causes: (1) the effect is due to segregation of dopants at grain boundaries, an effect becoming less important at larger grain sizes; or (2) the change reflects a change in the average nature of the grain boundaries, grain boundaries at small ds being a set of high- and low-energy boundaries with all kinds of misfit, those at large grain sizes consisting largely of low-energy boundaries, the high-energy boundaries having disappeared during recrystallization. Obviously the properties of low-energy boundaries more closely resemble bulk properties than those of high-energy boundaries do.

3.2. Compressive creep

Creep rate depends on self-diffusion coefficients which may depend on oxygen pressure, temperature, and doping [5] and are expected to be different for the bulk of grains and grain boundaries, and depend on stress, s, and grain size, d, with exponents n and m that are typical for the mechanism. It is, therefore, necessary to measure the dependence on all these variables if one wishes to determine mechanisms and their characteristic parameters. Fig. 12 shows the stress dependence of undoped samples with grain sizes $d = 3\,\mu$m and $\geqslant 100\,\mu$m. The exponent $n = 2.7$ found for the large-grain sample indicates a dislocation mechanism, either viscous glide or climb, for which, $n = 3$ [19, 20] is expected at large grain sizes [3]. A similar observation was made by Lessing and Gordon [4]. The value $n = 1.3$ found for the small grain sample is somewhat larger than expected for Nabarro–Herring creep which requires $n = 1$. The excess may be due to experimental scatter or to a contribution by boundary sliding [21]. Fig. 13 shows the stress dependence for samples doped with 500 and 5000 ppm Fe which have stress exponents $n = 1.25$ and 1.05. Fig. 14 shows the

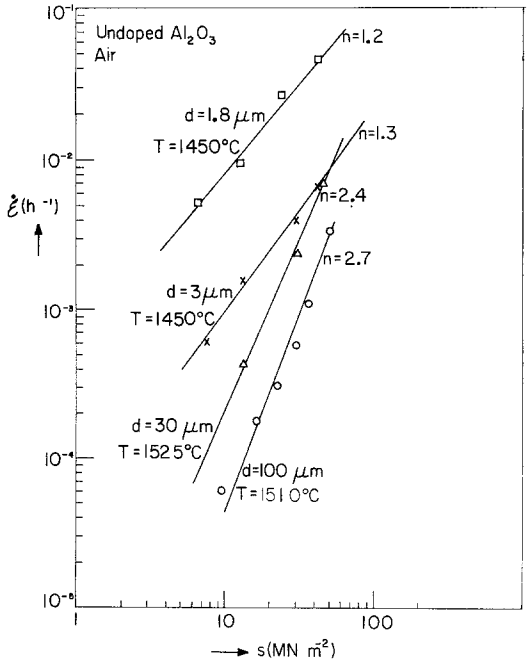

Figure 12 Stress dependence of creep rate for undoped Al_2O_3 with grain size 3 μm at 1450° C, and >100 μm, $T = 1510°$ C, both in air.

grain-size dependence for undoped samples in air under a stress of 7.5 MN m^{-2} at 1500° C. It is limited by the Nabarro–Herring mechanism (bulk

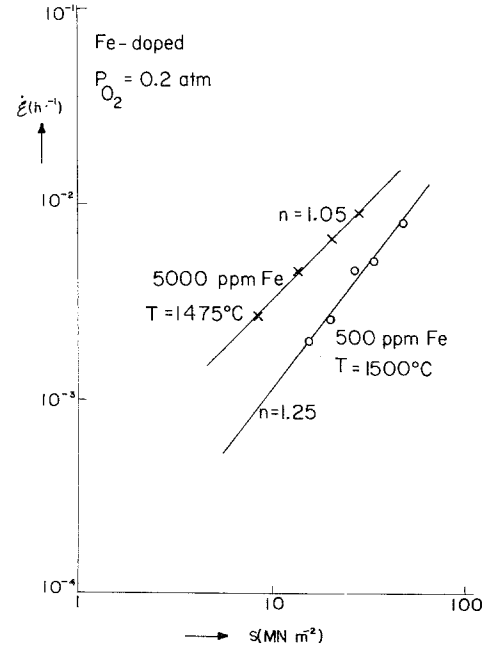

Figure 13 Stress dependence of creep rate for Al_2O_3 doped with 500 ppm Fe, $T = 1500°$ C, $d = 3$ μm, and 5000 ppm Fe, $T = 1475°$ C, $d = 10$ μm, both in air

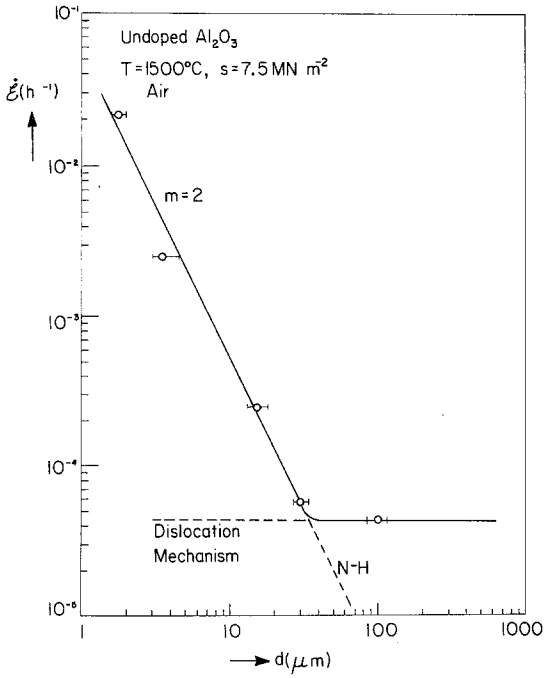

Figure 14 Grain-size dependence of creep rate for undoped Al_2O_3 in air at 1500° C under a stress of 7.5 MN m^{-2} and the calculated contribution by the Nabarro–Herring mechanism.

diffusion control, d-exponent, $m = 2$) at grain sizes <100 μm. Independence of d at $d > 100$ μm indicates a dislocation mechanism, as concluded earlier from the stress dependence (Fig. 12).

The dashed line in Fig. 14 was calculated for Nabarro–Herring creep with [1]

$$\dot{\epsilon}_{NH} = 13.3 \frac{\Omega_v D_b s}{kTd^2}, \qquad (3)$$

where Ω_v, the molar volume of Al_2O_3, is 4.2×10^{-23} cm^3 and D_b, the bulk self-diffusion coefficient of the rate limiting species, is equal to 7.14×10^{-13} cm^2 sec^{-1}. With an average observed activation energy of 6.07 eV (Fig. 16),

$$D_b = 1.5 \times 10^5 \exp\left(-6.07 \frac{eV}{kT}\right) \text{cm}^2 \text{ sec}^{-1} \qquad (4)$$

close to the expression

$$D_b = 1.35 \times 10^5 \exp\left(-5.96 \frac{eV}{kT}\right) \text{cm}^2 \text{ sec}^{-1} \qquad (5)$$

is valid for Al_2O_3 saturated with MgO [23].

Fig. 15 shows the p_{O_2} dependence of the creep rate for an undoped sample ($d = 100$ μm) and 5000 ppm Fe ($d = 10$ μm), all at temperatures

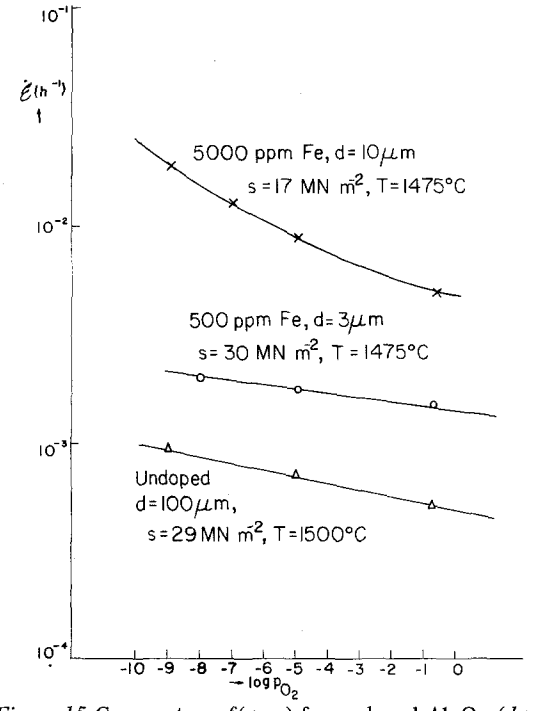

Figure 15 Creep rate as $f(p_{O_2})$ for undoped Al_2O_3 ($d \approx 100\,\mu m$, $s = 29\,MN\,m^{-2}$, $T = 1500°\,C$); Al_2O_3 : 500 ppm Fe ($d = 3\,\mu m$, $s = 30\,MN\,m^{-2}$, $T = 1475°\,C$); Al_2O_3 : 5000 ppm Fe ($d = 10\,\mu m$, $s = 17\,MN\,m^{-2}$, $T = 1475°\,C$).

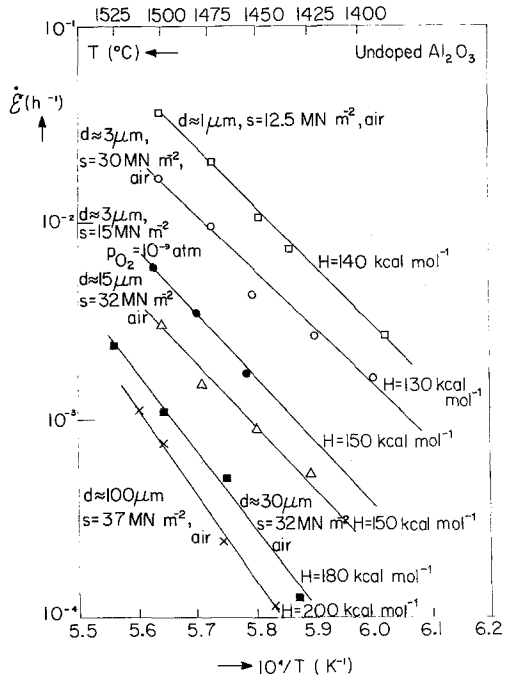

Figure 16 Temperature dependence of the creep rate for undoped Al_2O_3 with $d = 3$, 20 and 100 μm under stresses of 30, 32 and 37 $MN\,m^{-2}$ in air and 10^{-7} atm O_2.

close to 1500° C. The p_{O_2} dependence of the former two samples is very weak, just as found for the ionic conductivity (Figs. 1 and 4). For the 5000 ppm Fe sample it is somewhat stronger, $\propto p_{O_2}^{0.06}$, not too different from the conductivity dependence $\propto p_{O_2}^{0.1}$, but still much weaker than the dependence expected for a sample dominated by Fe. No doubt this is caused by the presence of $\simeq 2.5 \times 10^{18}$ fixed valency acceptor (Mg, Ca) in addition to the Fe. Fig. 16 shows the temperature dependence of the creep rate of undoped samples of various grain sizes at different oxygen pressures. The small grain size samples ($d = 3$ and 20 μm) with Nabarro–Herring creep have activation energies of 5.64 and 6.51 eV at high p_{O_2}, and 6.5 eV ($d = 2\,\mu m$) at low p_{O_2}. The large grain sample ($d = 100\,\mu m$) with creep by dislocation climb or viscous glide has an activation energy of 8.16 eV. Fig. 17 shows the temperature dependence of creep by Nabarro–Herring mechanism for Fe-doped samples at different oxygen pressures. The activation energies are 4.77 and 6.07 eV at high p_{O_2} and 4.12 and 5.64 at low p_{O_2}. Thus, for Nabarro–Herring creep the activation energies vary from 4.8 to 6.1 eV at high p_{O_2} and from 4.12 to 6.5 eV at low p_{O_2}, while for

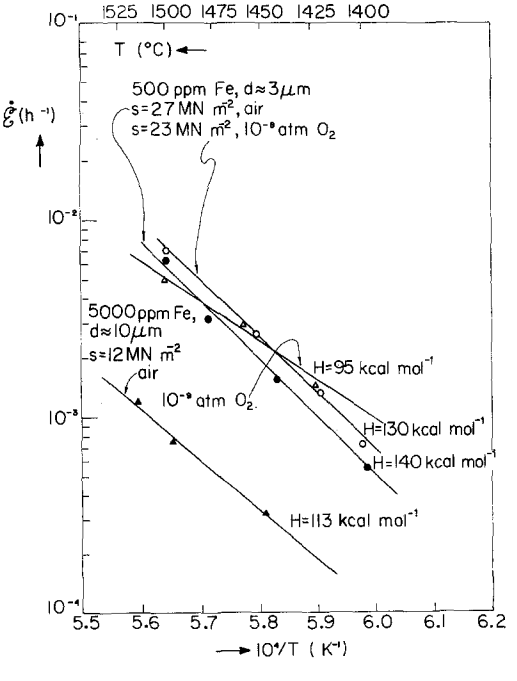

Figure 17 Temperature dependence of creep rate for Fe-doped Al_2O_3. 500 ppm Fe, density 99%, $d = 3\,\mu m$, $s = 27\,MN\,m^{-2}$, air, and $s = 23\,MN\,m^{-2}$, 10^{-8} atm O_2. 5000 ppm Fe, density 97%, $d = 10\,\mu m$, $s = 20\,MN\,m^{-2}$ air and 10^{-9} atm O_2.

the dislocation mechanism, the activation energy is 8.7 eV. Similar values have been reported for the latter by other authors, e.g. 8.0 ± 4.0 eV [20, 23], 7.8 eV [24], or 8.6 eV [25] However, this correspondence may be fortuitous, the latter values including the enthalpy of formation of defects whereas our values do so not at all or to a smaller extent.

4. Discussion

Table III shows activation energies for ionic and electronic (hole) conductivity and creep.

The activation energies of creep are in reasonable agreement with values from 5.5 to 6.5 eV reported by Lessing and Gordon [4] for pure Al_2O_3 and Al_2O_3 doped with Fe or Cr. All creep values are appreciable larger than the values 3.3 to 4.4 eV found for σ_i.

The activation energy of creep in the region dominated by a dislocation mechanism is still larger (8.7 eV). According to the normally accepted model, the rate-limiting step in the Nabarro–Herring mechanism of creep is bulk diffusion of Al, oxygen transport by grain-boundary diffusion being faster. The latter conclusion is based primarily on oxygen self-diffusion measurements by Oishi and Kingery [26]. As shown earlier, the lack of a decrease of σ_i with increasing d indicates that there is no fast grain-boundary transport of either oxygen or aluminium ions in acceptor dominated samples. Yet fast grain-boundary diffusion by neutral oxygen is still possible. In the presence of such oxygen transport, the aluminium transport through the bulk must be either by a neutral species (which may be ruled out for we observe ionic conduction) or by ambipolar diffusion of charged ionic and electronic species, Al_i^{3+} and h^+. Ambipolar diffusion of charged Al and O species could also occur, but in this case both Al and O would be transported through the bulk and no grain-boundary diffusion of oxygen would be involved.

TABLE III Activation energies of conduction and creep (eV)

Sample	d (μm)	Creep (s = 2037 MN m^{-2})		σ_i	σ_h
		air	10^{-9} atm O_2		
undoped	3	5.64	6.50	3.8	1.9
	10			3.4	2.3
	20	6.50			
	100	8.77		4.0	2.3
+ 500 ppm Fe	3	6.07	5.64	4.4	3.1
	10			3.9	2.9
+ 5000 ppm Fe	10	4.77	4.12	3.7	2.9

Following the standard approach to ambipolar diffusion of Al_i^{3+} and h^+ [28], with $[h^+] = \alpha[Al_i^{2+}]$, $\alpha = f(p_{O_2}, T)$ and assuming $9[Al_i^{3+}] \gg [h]$, one finds

$$(D_{Al})_b \equiv D(Al_i^{3+})_{eff}[Al_i^{3+}] = \frac{kT}{3Nq^2}\frac{\sigma_{Al}\sigma_h}{\sigma_{Al}+\sigma_h}$$

$$= \frac{3D(Al_i^{3+})D(h^+)[Al_i^{3+}][h^+]}{9D(Al_i^{3+})[Al_i^{3+}] + D(h^+)[h^+]}. \quad (6)$$

For $\sigma_h \gg \sigma_{Al}$ this expression reduces to

$$(D_{Al})_b = 3D(Al_i^{3+})[Al_i^{3+}] = \frac{kT}{3Nq^2}\sigma_{Al}, \quad (7)$$

and for $\sigma_{Al} \gg \sigma_h$, to

$$(D_{Al})_b = \tfrac{1}{3}D_h[h^+] = \frac{kT}{3Nq^2}\sigma_h. \quad (8)$$

Our conductivity experiments have shown that $\sigma_h \geqslant \sigma_i$ at large p_{O_2} while $\sigma_h \ll \sigma_i$ at $p_{O_2} = 10^{-9}$ atm. Therefore, if there is fast transport of neutral oxygen along grain boundaries, there might be a different temperature dependence of the creep rate at high and low p_{O_2}, the activation energy in the latter situation approaching that of hole conduction (see Equation 5). Although Table III reveals some differences in the activation energy of creep at high and low p_{O_2}, these differences are not consistent, and appear to be within the margin of error. And in no case does the activation energy of creep come close to that of hole conduction. Let us see whether it is possible to find a model on the basis of which experimental results can be explained if fast grain-boundary diffusion by neutral oxygen is assumed to occur. Table IV shows the dependence of defect concentrations in Al_2O_3 : Mg and Al_2O_3 : Fe on oxygen pressure and dopant concentration arrived at on the basis of two defect models: one, (I), (dominated by $[A^-] = 2[V_O^{2+}]$), the other, II, dominated by $[A^-] = 3[Al_i^{3+}]$. Model I is to be expected if the basic ionic disorder mechanisms in Al_2O_3 is Schottky disorder as proposed recently [29]. Model II is to be expected if Frenkel disorder of Al^{3+} is the dominant basic ionic disorder mechanism. It can, however, also occur if Schottky disorder is dominant provided $[A^-] > 8/9\,K_S/K_F^2$, K_S and K_F being the mass

TABLE IV Oxygen pressure and dopant-concentration dependence for various defects in various point defect models; [ ] = concentration in mole fractions

Model neutrality condition →		I $[A^-] \sim 2[V_O^{2+}] > 3[Al_i^{3+}]$	II $[A^-] \sim 3[Al_i^{3+}] > 2[V_O^{2+}]$
$A \equiv Mg_{Al}$			
	$[V_O^{2+}]$	$^{1/2}[A^-] \sim {}^{1/2}[A]_{total}$	$3^{-2/3} K_S^{1/3} K_F^{-2/3} [A]_{total}^{2/3}$
	$[V_{Al}'']$	$2^{-3/2} K_S^{1/2} [A]_{total}^{-3/2}$	$3K_F [A]_{total}^{-1}$
	$[Al_i^{3+}]$	$2^{3/2} K_F K_S^{-1/2} [A]_{total}^{3/2}$	$1/3[A]' \sim 1/3[A]_{total}$
	$[h^+]$	$2^{-1/2} K_V^{1/2} [A]_{total}^{1/2} p_{O_2}^{1/4}$	$3^{-1/3} K_V^{1/2} K_S^{1/6} K_F^{-1/3} [A]_{total}^{1/3} p_{O_2}^{1/4}$
$A \equiv Fe_{Al}$			
	$[Fe_{Al}^x]$	$[A]_{total}$	$[A]_{total}$
	$[V_O^{2+}]$	$4^{1/3} (K_{ox.V}^A)^{1/3} [A]_{total}^{2/3} p_{O_2}^{-1/6}$	$3^{1/2} K_F^{-2/3} (K_{ox.i}^A)^{-1/12} [A]_{total}^{1/2} p_{O_2}^{-1/8}$
	$[V_{Al}^{3-}]$	$1/2 K_S^{1/2} (K_{ox.V}^A)^{1/2} [A]_{total}^{-1} p_{O_2}^{-1/4}$	$3^{-3/4} K_F (K_{ox.i}^A)^{1/8} [A]_{total}^{-3/4} p_{O_2}^{3/16}$
	$[Al_i^{3+}]$	$2K_F K_S^{-1/2} (K_{ox.V}^A)^{-1/2} [A]_{total} p_{O_2}^{-1/4}$	$3^{3/4} (K_{ox.i}^A)^{-1/8} [A]_{total}^{3/4} p_{O_2}^{-3/16}$
	$[h^+]$	$2^{1/3} K_V^{1/2} (K_{ox.V}^A)^{-1/6} [A]_{total}^{1/3} p_{O_2}^{1/6}$	$3^{1/4} K_V^{1/2} K_F^{-1/3} (K_{ox.i}^A)^{-1/24} [A]_{total}^{1/4} p_{O_2}^{3/16}$
		$K_F = [V_{Al}^{3+}][Al_i^{3+}]$	$K_S = [V_{Al}^{3+}]^2 [V_O^{3+}]^3$
		$^{1/2}O_2 + V_O^{2+} + 2A_{Al}^- \rightleftarrows O_O^x + 2A_{Al}^x; K_{ox.V}^A$	
		$2Al_i^{3+} + 6A_{Al}^- + {}^{3/2}O_2^2 \rightleftarrows Al_2O_3 + 6A_{Al}^x; K_{ox.i}^A$	
		$^{1/2}O_2 + V_O^{2+} \rightleftarrows O_O^x + 2h^+; K_V$	

action equilibrium constants of Schottky and Frenkel disorder.

The two models can each give rise to four situations with respect to the relative magnitude of the various partial conductivities. These are sketched in Figs. 18 and 19 for $A \equiv Mg$. Tables V and VI sum up the essential features of the variants, all judged on the basis of the assumption that there is fast oxygen transport along grain boundaries by a neutral species, so that the ionic species limiting creep must be Al_i^{3+}. Starting with Model I (Fig. 18, Table V) it is seen that Ia explains the absence of a creep-rate dependence on σ_h because $\sigma(Al^{3+}) < \sigma(h^+)$ at all p_{O_2}. The establishment of this inequality is helped by the fact that the activation energy of σ_h is smaller than that of $\sigma(Al_i^{3+})$ i.e. that of the creep rate).

Model I has $\mu(V_O^{3+}) > \mu(Al_i^{3+})$ and $H(V_O^{2+})_{mob} = 2.75\,eV < H(Al_i^{3+})_{mob} = 4.65\,eV$. The former value is close to $H(O)_{mob} = 2.52\,eV$ reported for single crystal Al_2O_3 by Oishi and Kingery [26]. Observed activation energies of σ_i ($\equiv \sigma_{Al}$ in model Ia) at constant composition are on the average larger: 2.84 eV (Al_2O_3 : Fe) [7], 3.97 eV (Al_2O_3 : Co) [6], 4.6 eV (Al_2O_3 : Mg) [8], 3.6 and 4.7 eV (unknown acceptors) [30] and 3.78 eV (Al_2O_3 : Mg, present paper), all close to the value calculated for Al_i^{3+} [29]. Although equality of activation energies of mobility for V_O^{2+} and Al_i^{3+} is acceptable for model Ia, it would also fit models Ib, c and d. These, however, all can be rejected on the basis of the fact that they all predict creep limitation by σ_h at low p_{O_2} – which is not observed. A similar

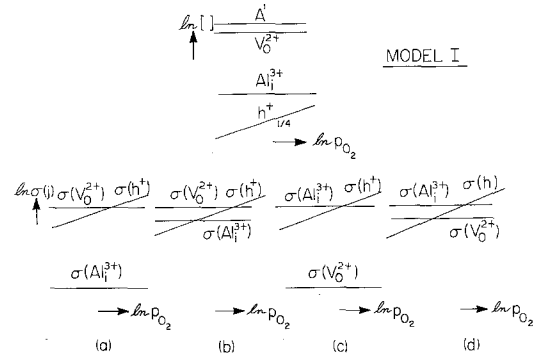

Figure 18 Defect isotherms for model I and four possible corresponding conductivity isotherms for Al_2O_3 : A with $A \equiv Mg$.

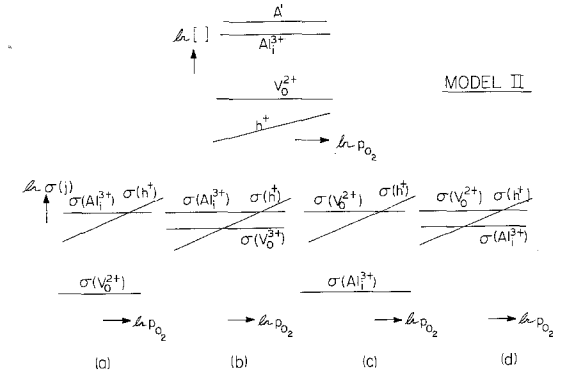

Figure 19 Defect isotherms for model II and four possible corresponding conductivity isotherms for Al_2O_3 : A with $A \equiv Mg$.

TABLE V Properties of various variants of model I depicted in Fig. 18a to d, for conductivity and creep rate in Al_2O_3 : A with A ≡ Mg with fast grain-boundary migration of oxygen as neutral species

	$[A^-] = 2[V_O^{2+}] > 3[Al_i^{3+}]$			
	Ia	Ib	Ic	Id
$\mu(V_O^{2+})/\mu(Al_i^{3+})$	$\geqslant 1$	$\leqslant 1$	$\ll 1$	< 1
$H(V_O^{2+})_{mob}/H(Al_i^{3+})_{mob}$	$\leqslant 1$	$\geqslant 1$	> 1	> 1
$\sigma(V_O^{2+})/\sigma(Al_i^{3+})$	$\gg 1$	> 1	$\gg 1$	> 1
σ_i	$\sigma(V_O^{2+})$	$\sigma(V_O^{2+}$	$\sigma(Al_i^{3+})$	$\sigma(Al_i^{3+})$
$\sigma(h^+)/\sigma(V_O^{2+})$	$< 1(p)^*; > 1(P)^\dagger$	$< 1(p); > 1(P)$	> 1	$< 1(p); > 1(P)$
$\sigma(h^+)/\sigma(Al_i^{3+})$	> 1	$< 1(p); > 1(P)$	$< 1(p); > 1(P)$	$< 1(p); > 1(P)$
Creep limitation	Al_i^{3+}	$h^+(p); Al_i^{3+}(P)$	Al_i^{3+}	$h^+(p); Al_i^{3+}(P)$
Agreement with calc. H_{mob} [29]	+	—	—	—
Agreement with observed H_{mob}	±	—	—	—

*p = small p_{O_2} ; †P = large p_{O_2}

consideration of models II (Fig. 19, Table VI) shows that IIa, b and d have to be rejected because they also require creep limitation by σ_h at low p_{O_2}. Model IIc is acceptable. Thus we are left with two acceptable models: Ia and IIc. These two models are, in fact, similar, differing only in their origin from different models. Models similar to Ia and IIc can be constructed for Al_2O_3 : Fe, the main difference being that for these the concentrations of A^- are $f(p_{O_2})$. The Fe equivalent of model Ia is to be preferred over that of IIc because it gives a better agreement for the p_{O_2}-dependence of the creep rate in Al_2O_3 : Fe reported by Hollenberg and Gordon [5] (see [28]). An objection against both Ia and IIc is the fact that it requires $D(O) > D(Al)$, while the work of Oishi and Kingery [26] and Paladino and Kingery [31] shows that $D(O) < D(Al)$. It is not clear, however, why if $H(V_O^{2+}) \leqslant H(Al_i^{3+})$, $D(O) < D(Al)$. A possible explanation is that the materials on which $D(O)$ and $D(Al)$ were measured contained different concentrations of impurities, the difference resulting from these. Let us now see whether the experimental results quantitatively fit the preferred model. The ionic conductivity of the undoped samples with $d \geqslant 20\,\mu m$ can be represented by

$$\sigma_i = 2.5 \times 10^5 \exp(-3.9\,eV/kT)\,\Omega^{-1}\,cm^{-1}. \quad (9)$$

From this we obtain

$$D(V_O^{2+})\,[V_O^{2+}] = \frac{kT\sigma_i}{N_O Z^2 q^2} = 2.67 \exp(-4.07\,eV/kT)\,cm^2\,sec^{-1}. \quad (10)$$

TABLE VI Properties of various variants of model II (depicted in Fig. 19a to d) for conductivity and creep in Al_2O_3 : A with A ≡ Mg with fast grain-boundary migration of oxygen as neutral species

	$[A'] = 3[Al_i^{3+}] > 2[V_O^{2+}]$			
	IIa	IIb	IIc	IId
$\mu(V_O^{2+})/\mu(Al_i^{3+})$	$\leqslant 1$	$\geqslant 1$	$\gg 1$	> 1
$H(V_O^{2+})_{mob}/H(Al_i^{3+})_{mob}$	$\geqslant 1$	$\leqslant 1$	< 1	< 1
$\sigma(V_O^{2+})/\sigma(Al_i^{3+})$	$\ll 1$	< 1	$\gg 1$	> 1
σ_i	$\sigma(Al_i^{3+})$	$\sigma(Al_i^{3+})$	$\sigma(V_O^{2+})$	$\sigma(V_O^{2+})$
$\sigma(h^+)/\sigma(V_O^{2+})$	> 1	$< 1(p); > 1(P)$	$< 1(p); > 1(P)$	$< 1(p); > 1(P)$
$\sigma(h^+)/\sigma(Al_i^{3+})$	$< 1(p)^*; > 1(P)^\dagger$	$< 1(p); > 1(P)$	> 1	$< 1(p); > 1(P)$
Creep limitation	$h^+(p); Al_i^{3+}(P)$	$h^+(p); Al_i^{3+}(P)$	Al_i^{3+}	$h^+(p); Al_i^{3+}(P)$
Agreement with calc. H_{mob} [29]	—	+	+	+
Agreement with observed H_{mob}	—	+	+	+

*p ≡ small p_{O_2} ; †P ≡ large p_{O_2}

Here $T \equiv 5.54 \times 10^3 \exp(-0.17\,eV/kT)$; $N_O = 7 \times 10^{22}$ cm^{-3} is the concentration of oxygen atoms in Al_2O_3; Zq is the charge per V_O defect, 3.2×10^{-19} C. Calculation of the self-diffusion coefficients of Al and O at 1500° C from Equations 4 and 10 yields the values 8.1×10^{-3} and 7×10^{-12} cm^2 sec^{-1}. Thus indeed $D(Al_i^{3+})[Al_i^{3+}] < D(V_O^{2+})[V_O^{2+}]$ as required for model Ia. The neutral oxygen species involved in the fast grain-boundary diffusion may be O_i^x or $(O_2)_i^x$. The concentration of the former would be $\propto p_{O_2}^{1/2}$, that of the latter $\propto p_{O_2}$, similar dependences being expected for $D(O)_{gb}$. The chance that the grain-boundary diffusivity remains fast relative to the bulk processes with a reduction of p_{O_2} over 9 orders of magnitude is evidently much greater for O_i^x than for $(O_2)_i^x$. Therefore, it is likely that O_i^x is the diffusing species. Corresponding species X_i^x have been found to be responsible for self diffusion in the bulk of III-V and II-VI compounds MX [32–35]. Hayes *et al.* [36] found oxygen permeation along grain boundaries in polycrystalline Al_2O_3 tubes $\propto p_{O_2}^{\frac{1}{2}}$.

There still is the need to explain the large activation energy, 8.7 eV, of creep by a dislocation mechanism. If the lower activation energies observed for Nabarro–Herring creep and σ_i are due to Al and O as suggested above, then the dislocation mechanism cannot be limited by diffusion of one of these species, i.e. it cannot be climb. Yet similar values have been reported for oxygen bulk diffusion, namely 6.6 ± 1.1 eV [26] and 7.7 eV [37]. It should be remembered, however, that the latter values were found at high temperatures and include the defect formation energy, the activation energy of mobility being only 2.5 eV [26], whereas our values contain defect formation energies to a smaller extent, if at all.

It is possible that the dislocation mechanism involves viscous glide rather than climb with a rate limited by diffusion of impurities (in our case, Mg). Yet the activation energy of diffusion of Ni^{2+} in Al_2O_3, an ion similar to Mg^{2+}, is only 4.5 eV [38], only half the required value. Finally problems arise in relation to differences in the grain-boundary diffusivities of oxygen reported by various authors. Lessing and Gordon [4] attribute these differences to doping. However, if the oxygen species involved in grain-boundary diffusion is neutral as we assume it to be, doping should have no effect. In fact, the values found from the creep rate of samples with different amounts of iron are very close, but all are markedly larger than values deduced by Mistler from the rate of sintering of undoped Al_2O_3 [4]. Lessing and Gordon [4] based their calculations on the observation of a gradual change of the grain-size exponent of the creep rate with increasing iron content from $n = 1.8$ in pure Al_2O_3 to $n = 2.98$ in strongly iron-doped Al_2O_3 which they explained as a transition from Nabarro–Herring creep with Al bulk limitation to Coble creep with oxygen-boundary limitation. It is possible that this explanation is not correct. We are investigating the possibility that the change in n with doping results from a redistribution of dopant over grain boundaries and bulk with changing grain size which, in turn, leads to a variation of D_b and D_{gb} with grain size to an extent dependent on the doping concentration. In the usual approach D_b and D_{gb} are assumed to be independent of grain size. If such a redistribution occurs it will also vary with temperature and, therefore, will make itself felt in the activation energies of conductivity and creep.

So far it has been shown that a model based on the assumption of fast oxygen grain-boundary diffusion can account for most of the observations. Yet the existence of such fast oxygen diffusion has not yet been clearly proven. If fast grain-boundary diffusion by oxygen should prove to be absent, models Ia and IIc could still explain most effects, the role of fast grain boundary diffusion being taken over by the bulk diffusion of V_O^{2+}. Different explanations then should have to be given for changes in the grain-size exponents in the expressions for the rate of creep and sintering, as already suggested above for the results of Lessing and Gordon [4].

Further experimental work is needed to check crucial results, in particular the ones that led to rejection of fast grain-boundary diffusion of oxygen ions and the possible dependence of the rate and activation energy of creep in the dislocation mechanism regime on the nature of dopants. In the theoretical field, the effect of changes in the dopant distribution with grain size should be investigated, while earlier single crystal work should be reanalysed taking into account the possibility that $[V_O^{2+}]\,\mu(V_O^{2+}) < [Al_i^{3+}]\,\mu(Al_i^{3+})$ even if $[V_O^{2+}] > [Al_i^{3+}]$, and vice versa.

5. Conclusions

Measurements of electronic and ionic conductivity and of creep rate as a function of p_{O_2}, T, grain

size, and stress for polycrystalline Al_2O_3 samples, undoped or doped with various concentrations of Fe and Ti leads to activation energies of conductivity and creep rate under various conditions. The results for the acceptor-dominated samples rule out fast diffusion by charged oxygen species. The results can be accounted for on the basis of a model in which there is fast transport of oxygen along grain boundaries by neutral species, probably O_i^x.

Acknowledgements

The authors gratefully acknowledge advice by T. G. Langdon and F. A. Mohamed of this laboratory in building up creep testing equipment, in performing creep measurements, and in interpretation of the results. This work was performed under contract with the United States Department of Energy, contract no. EY-76-03-0113, Project Agreement 27.

References

1. R. S. GORDON, *J. Amer. Ceram. Soc.* **56** (1973) 147.
2. *Idem*, in "Mass Transport Phenomena in Ceramics", edited by A. R. Cooper and A. H. Heuer (Plenum Press, New York, 1975) p. 445.
3. F. A. MOHAMED and T. G. LANGDON, *Met. Trans.* **5** (1974) 2339.
4. P. A. LESSING and R. S. GORDON, *J. Mater. Sci.* **12** (1977) 2291.
5. G. W. HOLLENBERG and R. S. GORDON, *J. Amer. Ceram. Soc.* **56** (1973) 140.
6. B. V. DUTT, J. P. HURRELL and F. A. KRÖGER, *ibid* **58** (1975) 421.
7. B. V. DUTT and F. A. KRÖGER, *ibid* **48** (1975) 474.
8. S. K. MOHAPATRA and F. A. KRÖGER, *ibid* **60** (1977) 141.
9. *Idem, ibid* **60** (1977) 381.
10. M. I. MENDELSON, *ibid* **52** (1969) 443.
11. J. YEE and F. A. KRÖGER, *ibid* **56** (1973) 189.
12. W. R. CANNON, thesis, Stanford University (1971).
13. W. C. JOHNSON and D. F. STEIN, *J. Amer. Ceram. Soc.* **58** (1975) 485.
14. R. I. TAYLOR, J. P. COAD and R. J. BROOK, *ibid* **57** (1974) 539.
15. S. S. C. TONG and J. P. WILLIAMS, *ibid* **53** (1970) 58.
16. R. I. TAYLOR, J. P. COAD and A. E. HUGHES, *ibid* **59** (1976) 374.
17. K. KITAZAWA and R. L. COBLE, *ibid* **57** (1974) 245.
18. O. T. ÖZKAN and A. J. MOULSON, *Brit. J. Appl. Phys. (J. Phys. D)* **3** (1970) 983.
19. F. R. N. NABARRO, *Phil. Mag.* **16** (1967) 231.
20. W. R. CANNON and O. D. SHERBY, *J. Amer. Ceram. Soc.* **56** (1973) 157.
21. W. R. CANNON and O. D. SHERBY, *ibid* **60** (1977) 44.
22. R. M. CANNON and R. L. COBLE, in "Deformation in Ceramic Materials", edited by B. C. Bradt and R. E. Tressler (Plenum Press, New York, 1975) pp. 61–100.
23. R. CHANG, *J. Appl. Phys.* **31** (1960) 484.
24. H. CONRAD, *J. Amer. Ceram. Soc.* **48** (1965) 195.
25. E. I. AKSELROD, I. I. VISNEVSKII, E. R. DOBROVINSKAYA and N. D. TALYANSKAYA, *Sov. Phys. Dokl.* **18** (1974) 683.
26. Y. OISHI and W. D. KINGERY, *J. Chem. Phys.* **33** (1960) 480.
27. F. A. KRÖGER, "The Chemistry of Imperfect Crystals", Vol. 3 (North-Holland, American Elsevier, New York, 1974) pp. 16–18.
28. S. K. MOHAPATRA and F. A. KRÖGER, *J. Amer. Ceram. Soc.* **61** (1978) 106.
29. G. J. DIENES, D. O. WELCH, C. R. FISCHER, R. D. HATCHER, O. LAZARETH and M. SAMBERG, *Phys. Rev.* **B11** (1975) 3060.
30. S. K. MOHAPATRA, S. TIKU and F. A. KRÖGER, *J. Amer. Ceram. Soc.* **62** (1979).
31. A. E. PALADINO and W. D. KINGERY, *J. Chem. Phys.* **37** (1962) 957.
32. M. S. SELTZER and J. B. WAGNER Jr, *J. Phys. Chem. Solids* **26** (1965) 233.
33. H. H. WOODBURY and R. B. HALL, *Phys. Rev.* **157** (1967) 641.
34. P. M. BORSENBERGER and D. A. STEVENSON, *J. Phys. Chem. Solids* **29** (1968) 1277.
35. V. KUMAR and F. A. KRÖGER, *J. Solid State Chem.* **3** (1971) 387.
36. D. HAYES, D. W. BUDWORTH and J. P. ROBERTS. *Trans. Brit. Ceram. Soc.* **62** (1963) 507.
37. D. J. REED and B. J. WUENSCH, *Amer. Ceram. Soc. Bull.* **56** (1977) 298, paper 101-B-77.
38. K. HIROTA and W. KOMATSU, *J. Amer. Ceram. Soc.* **60** (1977) 108.

Received 6 July and accepted 18 September 1978.